



UNIVERSIDADE DA BEIRA INTERIOR
Engenharia

A Comparison of Different Gas Turbine Engines Ground Vortex Flows

Pedro Alexandre Rodrigues Manquinho

Dissertação para obtenção do Grau de Mestre em
Eng. Aeronáutica
(2º ciclo de estudos)

Orientador: Prof. Doutor Jorge M. M. Barata
Co-orientador: Prof. Doutor André R. R. Silva

Covilhã, Outubro de 2010

Dedictory

This thesis is dedicated to my family, with particular attention to my mother who took me the first time to see a Public University if memory serves me right whit four or five years of age to my father who instilled in me a love for aviation and my lady who puts up whit me for many years.

Acknowledgment

Here, you would usually thank all who contributed to this work but I will thank all those who contributed to my academic growth, the Department of Aerospace Sciences, to all my teachers but of which I must mention two in particular, Professor. Dr. Jorge M. M. Barata my supervisor and the person I have in great esteem as a human being and academic and Prof. Dr. Andre R. R. Silva who I watched grow as academic with merit and great panache.

Resumo

O design do bocal de admissão do motor é muito importante porque, é um dos componentes do motor directamente em interface com o fluxo em torno do motor e o fluxo de ar interno. A admissão é projectada para dar a quantidade adequada de fluxo de ar necessário as condições de fluxo livre das condições exigidas na entrada do compressor com perda de pressão mínima pelo mecanismo. Quando as perdas de pressão e as distorções de fluxo são muito baixas, o desempenho do motor é ideal, e essa é a razão por que o fluxo de ar tem de ser tão uniforme quanto possível, ao compressor. Esta condição de fluxo de ar é necessária em todas as configurações de voo, inclusive quando a aeronave está manobrando nas tarefas de solo. O desempenho de admissão depende o fluxo de massa entregue para o compressor. O fluxo de massa interno permanece constante do tubo fluxo capturados para o rosto do compressor e supondo que o fluxo seja incompressíveis devido a velocidades de baixa velocidade, será dada por $A_i U_i = A_\infty U_\infty$. Uma vez que o fluxo de massa é constante e a relação da área está relacionada à proporção de contracção de tubo de fluxo, a

relação da área pode ser expresso como $\frac{A_\infty}{A_i} = \left(\frac{L_q}{D_i}\right)^2$. O rácio de captura A_∞ / A_i é controlado pelo motor, o fluxo de massa do motor, o diâmetro de admissão e a velocidade de fluxo livre. A área definida pelo limite entre o ar que entra no motor e o ar que não é chamada a área de admissão capturada. A taxa de fluxo e a forma de tubo de fluxo variam de acordo com as condições de operação do motor. Perto da configuração estática desde que o ar ambiente está em repouso, o motor acelerar o ar usando o máximo impulso. A aceleração local extrema do fluxo, o bordo de entrada pode levar à separação de fluxo de ar no presente region^{2, 3}. Configuração de crossflow, na forma do tubo do fluxo é modificada perto do bordo. O crossflow leva a um aumento da velocidade de fluxo perto do bordo dependendo da força das origens crossflow de alta velocidade na separação de fluxo, levando a uma perda total da pressão.

A formação de vórtices de solo depende da potência do motor, altura de admissão de velocidade e o mecanismo de vento e tamanho. Trabalhos publicados anteriores mostram que o fenómeno só pode ocorrer com a presença de uma linha de estagnação entre o solo e a admissão, de que depende do rácio de velocidade U_i / U_∞ e da altura não-dimensional do eixo motor acima do solo, h/d_i (Fig. 1). Em condições estáticas, o fluxo de ar de admissão exigem aumentos e a admissão captura superficial aumenta em diâmetro e começa a incluindo a terra para trazer o fluxo de ar necessário para a fan^{4, 5}. Normalmente a formação de vórtices de solo é caracterizada por baixa h/d_i e alta U_i / U_∞ que corresponde a um mecanismo de funcionamento junto ao solo em uma entrada elevada massa flow⁶. Assim, o mecanismo de formação de admissão é fortemente dependente da altura do eixo motor acima do solo, a taxa de velocidade e a presença de uma velocidade de upstream. Foram identificados quatro tipos diferentes das condições que conduzem à formação de vórtices de

solo. Pode ser gerado um vórtice sem vento ambiente e com uma baixa relação h/d_i (geralmente inferior a um). Devido à proximidade do solo, níveis elevados de sucção abaixo de admissão do motor leva a um forte fluxo debaixo da admissão. Nestas condições, é possível visualizar a admissão do motor e o terreno dois para cima vórtices espiral. Na condição de noventa, afigura-se que as duas vórtices são conversores, e a motricidade é induzida pela camada limite. É um fluxo de vento de frente, quando o ar é sugado para a admissão do motor, o campo de fluxo debaixo da admissão começa a fundir em duas vórtices conversores eretas e um fluxo rápido em direcção oposta do vento aparece entre eles. Para razões altas de velocidade (> 20) o sentido de rotação dos dois vórtices alterna para o mesmo mecanismo não-vento. Com um 90° crossflow dois tipos diferentes de vórtices aparecem em torno da admissão: um vórtice de entrada e um vórtice à direita.

Quando a admissão de motor está orientada em um ângulo de Guinada de 90° e com a presença de crossflow com upstream longe vorticidade vertical, há a formação de um vórtice único dentro da admissão. Neste caso, o sentido de rotação do vortex é oposto do ambiente vorticidade. Outros mecanismos de formação também existem e podem ser considerados como combinações os anteriores que levam a um grande número de combinações possíveis que são responsáveis para a necessidade de mais estudos compreender toda a física envolvida.

Ferramentas de CFD foram aplicadas recentemente para a compreensão do vortex com relativo sucesso. Nakayama & Jones¹⁰ usou métodos painel para simular a entrada e modos interação, notando que a velocidade do vento necessária para fundir o vórtice afastado era inferior a medida experimentalmente.

Barata et al.¹¹ relatório cálculos de Navier-Stokes e previu com êxito os fenómenos de vórtice de solo usando as condições operacionais reais para o caso do motor Trent 900. A formação de vórtice de solo no fluxo de ventos irrotational é analisada em detalhe para esta configuração, e a formação do vortex à direita foi associada a um fluxo muito complexo.

No presente livro, o trabalho anterior de Barata et al.¹¹ é estendido para incluir vários motores que estão sendo usados no presente. Os fluxos de vórtice de solo produzidos pelos motores diferentes são comparados e discutidos para cada condição operacional.

Palavras-chave

Admissão, vórtice, solo, fluxo, motor, vento cruzado.

Abstract

The design of an engine intake is very important because, it is one of the engine components that directly interface with the flow around the engine and the internal airflow. The inlet is designed to give the appropriate amount of airflow required from the free-stream conditions to the conditions required at the entrance of the compressor with minimal pressure loss by the engine¹. When the pressure losses and the flow distortions are very low, the performance of the engine is optimal, and that is the reason why the airflow has to be as uniform as possible when entering into the compressor. This airflow condition is necessary in all flight configurations including when the aircraft is maneuvering on ground tasks. The intake performance depends on the mass-flow delivered to the compressor. The internal mass-flow stays constant from the captured stream tube to the compressor face and assuming that the flow is incompressible due to low speed velocities, it will be given by $A_i U_i = A_\infty U_\infty$. Since the mass-flow is constant and the area ratio is related to the

stream tube contraction ratio, the area ratio can be expressed as $\frac{A_\infty}{A_i} = \left(\frac{L_q}{D_i}\right)^2$. The capture ratio A_∞ / A_i is controlled by the engine, the engine mass-flow, the inlet diameter and the free-stream velocity. The area defined by the boundary between the air that enters in the engine and the air that does not is called the intake captured area. The flow ratio and the stream-tube shape vary with the operation conditions of the aircraft engine. In near static configuration since the ambient air is at rest, the engine must accelerate the air using maximum thrust. The extreme local acceleration of the flow at the inlet lip can lead to airflow separation in this region^{2,3}. In cross-wind configuration, the shape of the stream tube is modified near the lip. The cross-flow leads to an increase in the flow velocity near the lip depending on the strength of the cross-flow, high velocity origins in flow separation leading to a total pressure loss at the engine fan.

The formation of ground vortices depends on engine power, wind velocity and engine inlet height and size. Previous published work show that the phenomenon can only occur with the presence of a stagnation streamline between the ground and the intake which is dependent on the velocity ratio U_i / U_∞ and the non-dimensional height of the engine axis above the ground, h / D_i (Fig. 1). In static conditions, the inlet airflow demand increases, and the inlet capture surface increases in diameter and starts including the ground to bring the necessary airflow to the fan^{4,5}. Typically the formation of ground vortices is characterized by low h / D_i and high U_i / U_∞ that corresponds to an engine operating close to the ground at a high inlet mass flow⁶. Hence, the mechanism of intake formation is strongly dependant of the height of the engine axis above the ground, the velocity ratio and the presence of an upstream velocity.

Four different types of conditions leading to the formation of inlet ground vortices have been identified. A vortex can be generated without ambient wind and with a low ratio h/D_i (typically less than one). Due to the ground proximity, high levels of suction beneath the engine inlet leads into a strong flow underneath the inlet upstream towards the intake lip⁷. In these conditions, it is possible to visualize at the engine intake and at the ground two upward spiraling vortices. Under no-wind condition, it appears that the two vortices are counter-rotating, and the vorticity is induced by the boundary layer. In a head-wind flow, when the air is sucked into the engine inlet, the flow field underneath the intake starts to roll up into two upright counter-rotating vortices and a fast flow into the opposite direction of the wind appears between them^{8,9}. For high velocity ratios (>20) the sense of rotation of the two vortices switches to the same as in the no-wind mechanism. With a 90° cross-wind two different kinds of vortices appear around the intake: an inlet vortex and a trailing vortex (Fig.3). When the engine intake is oriented at a 90° yaw angle and with the presence of cross-wind with far upstream vertical vorticity, there is the formation of a single vortex inside the intake. In this case the sense of rotation of the vortex is opposite to the ambient vorticity. Other mechanisms of formation also exist and can be considered as combinations of the previous ones that lead to a large number of possible combinations that are responsible for the need of more studies in order to understand all the physics involved.

CFD tools have been applied recently to the understanding of the ground vortex with relative success. Nakayama & Jones¹⁰ used panel methods to simulate the inlet and ground interaction, noting that the wind speed needed to blow the vortex away was lower than the measured experimentally. Barata et al.¹¹ report Navier-Stokes calculations and predicted successfully the ground vortex phenomena using real operational conditions for the case of the engine Trent 900. The ground vortex formation in irrotational crosswind flow is analyzed in detail for this configuration, and the formation of the trailing vortex was associated to a very complex flow.

In the present paper the previous work of Barata et al.¹¹ is extended to include several engines that are being used in the present. The ground vortex flows produced by different engines are compared and discussed for each operational condition.

Keywords

Intake, vortex, ground, flow, engine, cross-wind.

Índice

Dedictory.....	iii
Agradecimentos	Erro! Marcador não definido.
Resumo	vii
Palavras-chave	viii
Abstract.....	x
Keywords.....	xi
Chapter 1	1
Introduction.....	1
Chapter 2	4
Mathematical Model.....	4
Chapter 3	7
Results	7
Chapter 4	31
Conclusions.....	31
References	32

Nomenclature

A_i	=	intake area
A_∞	=	frequency of oscillation of the ground vortex
D_i	=	inner diameter of the intake
h	=	height of the engine axis above the ground
k	=	turbulent kinetic energy
L_q	=	intake stream tube length
\dot{m}	=	mass flow
U_i	=	intake throat velocity
U_∞	=	free stream velocity
V_∞	=	tangential velocity
Γ	=	vortex circulation
ζ	=	vorticity
ρ	=	density
μ	=	dynamic viscosity
ν	=	kinematic viscosity
ν_T	=	turbulent kinematic viscosity
ϕ	=	any dependent variable

Chapter 1

Introduction

The design of an engine intake is a very important part of the aircraft engine design because it influences the overall performance. The inlet is designed to give the appropriate amount of airflow required from the free-stream conditions to the conditions required at the entrance of the compressor with minimal pressure loss by the engine¹. Flow distortions at the inlet cause conditions that were not taken into account during the design process and usually represent a negative influence. So, to obtain the optimal engine conditions the airflow must be as uniform as possible when entering the compressor. This airflow condition is necessary in all flight configurations including when the aircraft is maneuvering on ground tasks where hazardous suction of objects may occur.

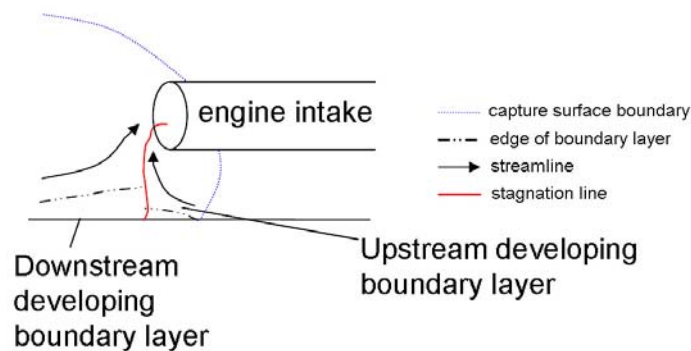


Figure 1. Ground vortex formation.

The intake performance depends on the mass-flow delivered to the compressor. The internal mass-flow stays constant from the captured stream tube to the compressor face and assuming that the flow is incompressible due to low speed velocities, it will be given by $A_i U_i = A_\infty U_\infty$. Since the mass-flow is constant and the area ratio is related to the stream tube contraction ratio, the

area ratio can be expressed as $\frac{A_\infty}{A_i} = \left(\frac{L_q}{D_i}\right)^2$. The capture ratio A_∞ / A_i is controlled by the engine, the engine mass-flow, the inlet diameter and the free-stream velocity. The area defined by the boundary between the air that enters in the engine and the air that does not is called the intake captured area. The flow ratio and the stream-tube shape vary with the operation conditions of the aircraft engine. In near static configuration since the ambient air is at rest, the engine must accelerate the air using maximum thrust. The extreme local acceleration of the flow at the inlet lip can lead to airflow separation in this region^{2,3}. In cross-wind configuration, the shape of the

stream tube is modified near the lip. The cross-flow leads to an increase in the flow velocity near the lip depending on the strength of the cross-flow, high velocity origins in flow separation leading to a total pressure loss at the engine fan.

The formation of ground vortices depends on engine power, wind velocity and engine inlet height and size. Previous published work show that the phenomenon can only occur with the presence of a stagnation streamline between the ground and the intake which is dependent on the velocity ratio U_i / U_∞ and the non-dimensional height of the engine axis above the ground, h/D_i (Fig. 1). In static conditions, the inlet airflow demand increases, and the inlet capture surface increases in diameter and starts including the ground to bring the necessary airflow to the fan^{4,5}. Typically the formation of ground vortices is characterized by low h/D_i and high U_i / U_∞ that corresponds to an engine operating close to the ground at a high inlet mass flow⁶. Hence, the mechanism of intake formation is strongly dependant of the height of the engine axis above the ground, the velocity ratio and the presence of an upstream velocity.

Four different types of conditions leading to the formation of inlet ground vortices have been identified. A vortex can be generated without ambient wind and with a low ratio h/D_i (typically less than one). Due to the ground proximity, high levels of suction beneath the engine inlet leads into a strong flow underneath the inlet upstream towards the intake lip⁷. In these conditions, it is possible to visualize at the engine intake and at the ground two upward spiraling vortices. Under no-wind condition, it appears that the two vortices are counter-rotating, and the vorticity is induced by the boundary layer. In a head-wind flow, when the air is sucked into the engine inlet, the flow field underneath the intake starts to roll up into two upright counter-rotating vortices and a fast flow into the opposite direction of the wind appears between them^{8,9}. For high velocity ratios (>20) the sense of rotation of the two vortices switches to the same as in the no-wind mechanism. With a 90° cross-wind two different kinds of vortices appear around the intake: an inlet vortex and a trailing vortex (Fig. 2). When the engine intake is oriented at a 90° yaw angle and with the presence of cross-wind with far upstream vertical vorticity, there is the formation of a single vortex inside the intake. In this case the sense of rotation of the vortex is opposite to the ambient vorticity.

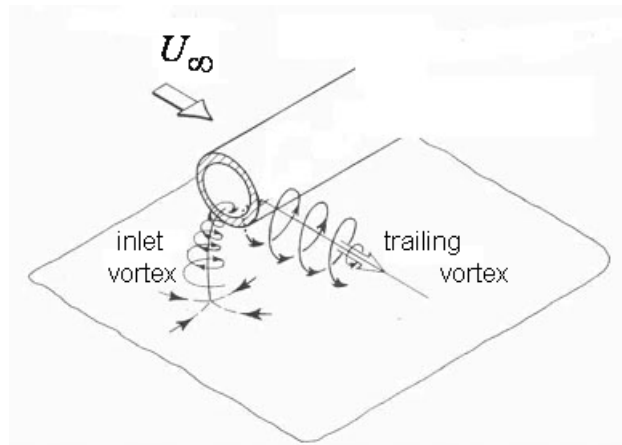


Figure 2. Sense of rotation of the inlet vortex and the trailing vortex (sketch adapted from Ref. 9).

Other mechanisms of formation also exist and can be considered as combinations of the previous ones that lead to a large number of possible combinations that are responsible for the need of more studies in order to understand all the physics involved. CFD tools have been applied recently to the understanding of the ground vortex with relative success. Nakayama & Jones¹⁰ used panel methods to simulate the inlet and ground interaction, noting that the wind speed needed to blow the vortex away was lower than the measured experimentally. Barata et al.¹¹ report Reynolds Averaged Navier-Stokes calculations and predicted successfully the ground vortex phenomena using real operational conditions for the case of the engine Trent 900. The ground vortex formation in irrotational crosswind flow is analyzed in detail for this configuration and engine, and the formation of the trailing vortex was associated to a very complex flow.

Chapter 2

Mathematical Model

The mathematical model used in the present study is described in detail in Ref. 11 and only the main features will be summarized here. The time averaged partial differential equations governing the steady, uniform-density isothermal three-dimensional flow

$$\rho \bar{U}_j \frac{\partial \bar{U}_i}{\partial X_j} = -\frac{\partial \bar{P}}{\partial X_i} + \frac{\partial}{\partial X_j} \left(\mu \frac{\partial \bar{U}_i}{\partial X_j} - \overline{\rho u'_i u'_j} \right) \quad (1)$$

and the continuity equation,

$$\rho \bar{U}_j \frac{\partial \bar{U}_i}{\partial X_i} = 0 \quad (2)$$

where solved together with the equations of transport of the turbulent kinetic energy and dissipation rate of the two-equation “ k - ε ” model¹⁰

$$\bar{U}_j \frac{\partial k}{\partial X_j} = \frac{\partial}{\partial X_j} \left(\frac{\nu_T}{\sigma_k} \frac{\partial k}{\partial X_j} \right) - \overline{u'_i u'_j} \frac{\partial \bar{U}_i}{\partial X_j} - \varepsilon \quad (5)$$

$$\bar{U}_j \frac{\partial \varepsilon}{\partial X_j} = \frac{\partial}{\partial X_j} \left(\frac{\nu_T}{\sigma_\varepsilon} \frac{\partial \varepsilon}{\partial X_j} \right) - C_1 \frac{\varepsilon}{k} \overline{u'_i u'_j} \frac{\partial \bar{U}_i}{\partial X_j} - C_2 \frac{\varepsilon^2}{k} \quad (6)$$

where C_1 and C_2 are additional dimensionless model constants, and σ_k and σ_ε are the turbulent Prandtl numbers for kinetic energy and turbulent dissipation.

The Reynolds stresses are expressed as

$$\overline{u'_i u'_j} = -\nu_T \left(\frac{\partial \bar{U}_i}{\partial X_j} + \frac{\partial \bar{U}_j}{\partial X_i} \right) + \frac{2}{3} k \delta_{ij} \quad (3)$$

where ν_T is the turbulence kinematic viscosity, which is derived from the turbulence model and expressed by $C_\mu k^2 / \varepsilon$.

The solution of the governing equations was obtained using a quadratic finite-difference method¹² that used discretized algebraic equations deduced from the exact differential equations that they represent.

The solution procedure is based on the SIMPLE algorithm widely used and reported in the literature (e.g. Ref. 13). It uses the staggered grid arrangement and a guess and correct procedure field such that the solution of the momentum equations satisfies continuity.

The computational domain has six boundaries where dependent values are specified: a free stream plane, a symmetry plane, and a solid wall. On the symmetry plane, the normal velocity vanishes, and the normal derivatives of the other variables are zero. At the solid surface, the wall function method¹⁴ is used to prescribe the boundary conditions for the velocity and turbulence quantities, assuming that the turbulence is in state of local equilibrium. The free stream plane is located at $Z=0$ and corresponds to the crossflow conditions. The engine intake boundary is represented by a right angled polygon and the mass flow rates and the momentum are matched to the experimental values. The intake represents a 1/1th scale model with a diameter that corresponds to each particular engine. The axis of the engine is located at a distance above the ground (h), which corresponds to the specific clearance distance. All the tests were performed for the case of irrotational crosswind, and the other conditions are shown in Table 1. The domain of solution, their dimensions and the system of axes are represented in Fig.3

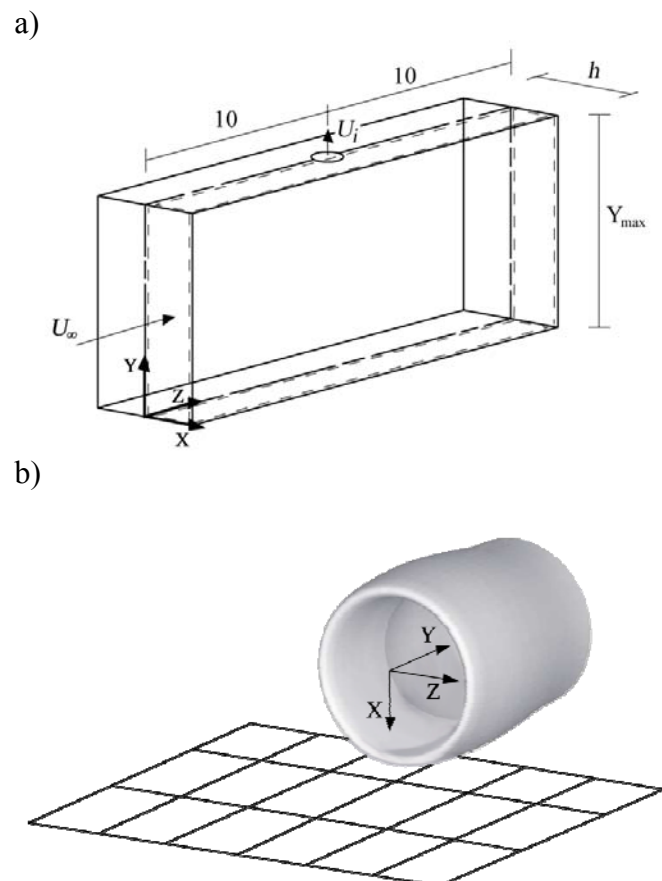


Figure 3. Domain of the solution a). Representation of the intake with referential at the center b).

Engine	Diameter (m)	Clearance Distance	Mass Flow (lb/s)	Mass Flow (Kg/s)	Radius (m)	Inlet Velocity (m/s)	H (m)
cf6-50	2,6670	0,8300	1450,0000	657,7089	1,3335	43,5947	2,1635
cf6-6	2,6670	0,8400	1300,0000	589,6701	1,3335	39,0849	2,1735
cf6-80a	2,6670	0,6540	1435,0000	650,9051	1,3335	43,1437	1,9875
cf6-80c2	2,6900	0,6500	1750,0000	793,7866	1,3450	51,7184	1,9950
cf6-80e1	2,6890	0,7600	1925,0000	873,1653	1,3445	56,9326	2,1045
cfm56-2	1,7350	0,5600	784,0000	355,6164	0,8675	55,6966	1,4275
cfm56-3	1,5240	0,4600	638,0000	289,3919	0,7620	58,7439	1,2220
cfm56-5a	1,7350	0,5800	816,0000	370,1314	0,8675	57,9700	1,4475
cfm56-5b	1,7350	0,5800	811,0000	367,8634	0,8675	57,6148	1,4475
cfm56-5c	1,8360	1,2200	1027,0000	465,8394	0,9180	65,1534	2,1380
cfm56-7	1,5490	0,4600	677,0000	307,0820	0,7745	60,3389	1,2345
rb211-535e4	1,8820	0,7400	1177,0000	533,8782	0,9410	71,0639	1,6810
trent 500	2,4740	0,4800	1897,0000	860,4647	1,2370	66,2796	1,7170
trent 700	2,4740	0,6900	2030,0000	920,7925	1,2370	70,9265	1,9270
trent 800	2,7940	1,0900	2378,0000	1078,6427	1,3970	65,1435	2,4870
trent 900	2,9460	1,0300	2655,0000	1204,2877	1,4730	65,4201	2,5030
trent 1000	2,8450	0,7100	2400,0000	1088,6217	1,4225	63,4101	2,1325
GE nx	2,8190	0,7400	2458,0000	1114,9300	1,4095	66,1460	2,1495

Table 1. Summary of selected engine characteristics.

Grid independence tests were performed with different mesh sizes, and the results for a mesh with 33×59×33 were found to be independent of numerical influences. Nevertheless, a finer grid of 49×89×49 meshes was used to give a better description of the engine inlet.

Chapter 3

Results

The ground vortex formation in irrotational crosswind flow is analyzed in the present section. In this configuration the ground vortex or inlet vortex that forms near the ground and is sucked by engine is accompanied by an additional feature which is the formation of the trailing vortex (see Fig. 2). This vortex develops from the lip of the inlet engine in the direction of the crossflow with its axis parallel to the ground.

Engine	XZ	YZ	3D	Nº of vortex	V_i/V_∞	H/Di
cf6-50	X			1	43,6863	0.97
cf6-6	X			3	39,1670	0.97
cf6-80a	X	X		2	43,2344	0.97
cf6-80c2				0	51,8271	0.97
cf6-80e1				0	57,0522	0.97
cfm56-2				0	55,8137	0.97
cfm56-3				0	58,8673	0.97
cfm56-5a	X			1	58,0918	0.97
cfm56-5b	X			1	57,7358	0.97
cfm56-5c				0	65,2903	0.97
cfm56-7	X			1	60,4657	0.97
rb211-535e4				0	71,2132	0.97
trent 500	X			1	66,4189	0.97
trent 700	X			1	71,0755	0.97
trent 800				0	65,2804	0.97
trent 1000				0	63,5434	0.97
GE nx				0	66,2850	0.97

Table 2. Summary of results for the selected conditions.

How can we see after a brief review of table 2 and for the conditions mentioned above ($V_i/V_\infty = \text{Max engine}$ and $H/Di = 0.97$) there are four sets of results obtained.

The largest group is the single vortex in the plane XZ which shows some examples

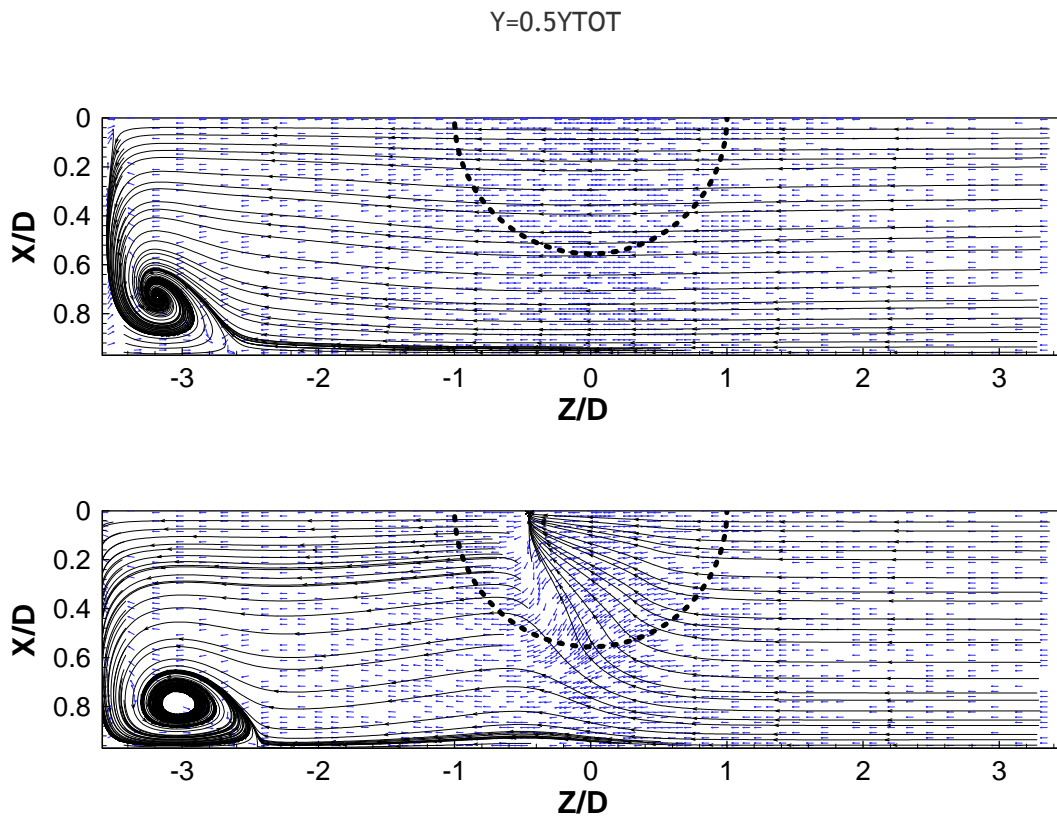


Figure 4. Engine Cf6-50 for U_i/U_∞ Max and $H/D_i=0.97$ $Y=0.95YTOT$

It is perfectly visible a ground vortex at position $X/D = 0.8$ $Z/D = -3$.

In the case of Figure 5 we can observe the same situation but on the opposite side of the stream

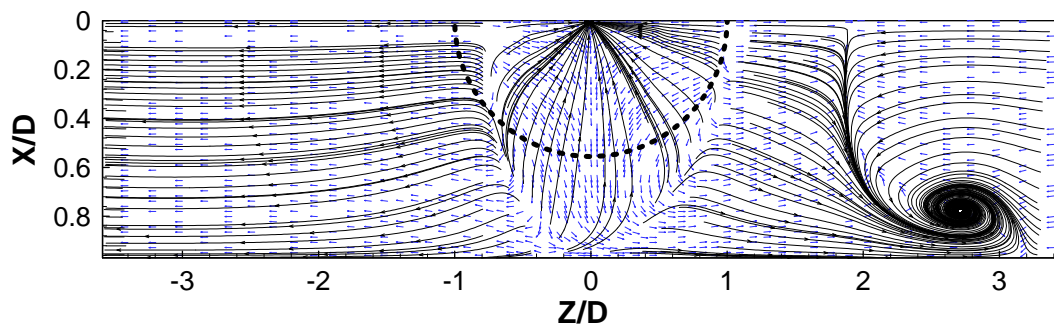


Figure 5. Engine Cfm56-7 for U_i/U_∞ Max and $H/D_i=0.97$, $Y=0.95YTOT$

Still in the group of single vortex engines, there is the situation of Trent 700 engine where the Vortex arises in a central position (Figure 6) and Trent 500 where this vortex in a higher position (Figure 7). It should be noted that the vortex of Figure 7 has a different sign (clockwise) which also applies in the Cfm56-5a.

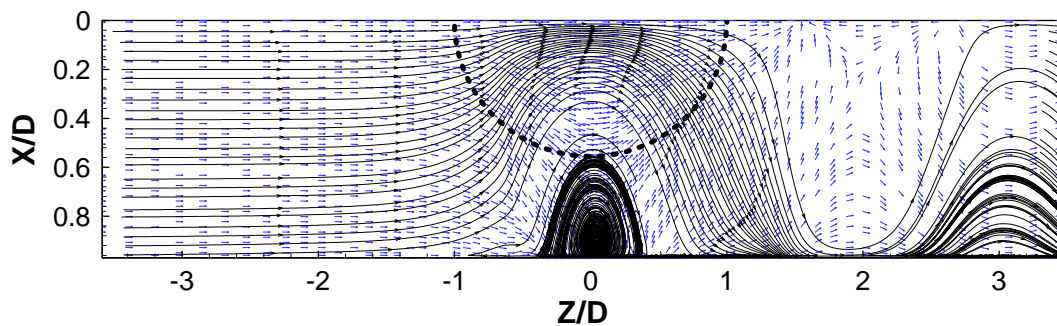


Figure 6. Engine Trent 700 for U_i/U_∞ Max and $H/D_i=0.97$, $Y=0.05Y_{TOT}$

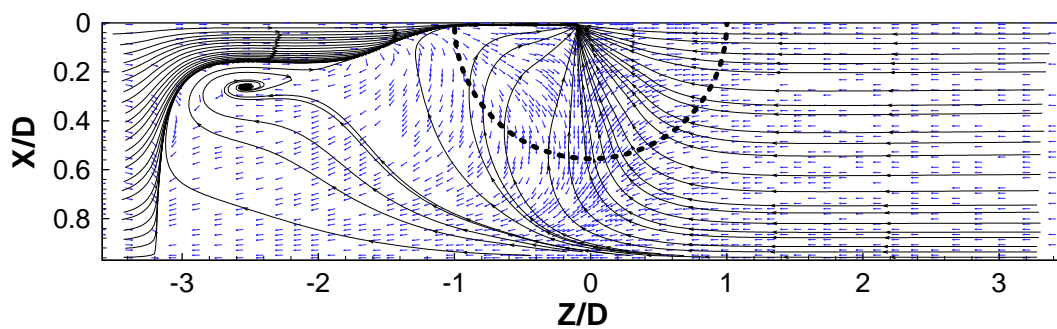


Figure 7. Engine Trent 500 for U_i/U_∞ Max and $H/D_i=0.97$, $Y=0.95Y_{TOT}$

In table 2 we can see two more vorticity situations. In the case of the Cf6-80a engine where there are two vorticity structures, one in the XZ plane and the other in YZ plane with can be seen in Figure 8 and Figure 9.

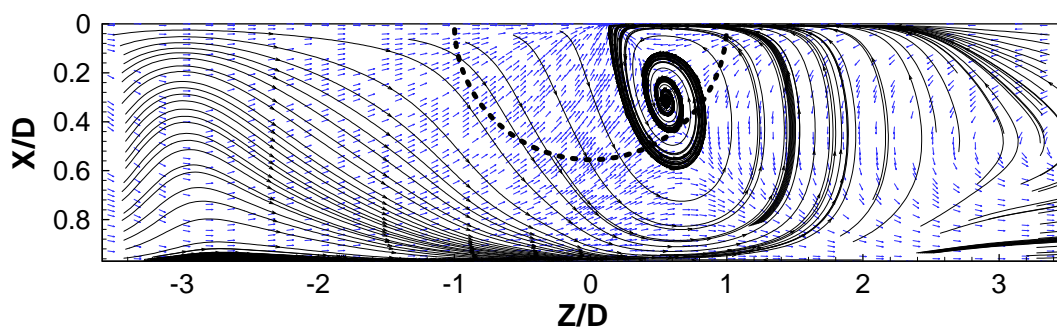


Figure 8. Engine Cf6-80a for U_i/U_∞ Max and $H/D_i=0.97$, $Y=0.05Y_{TOT}$

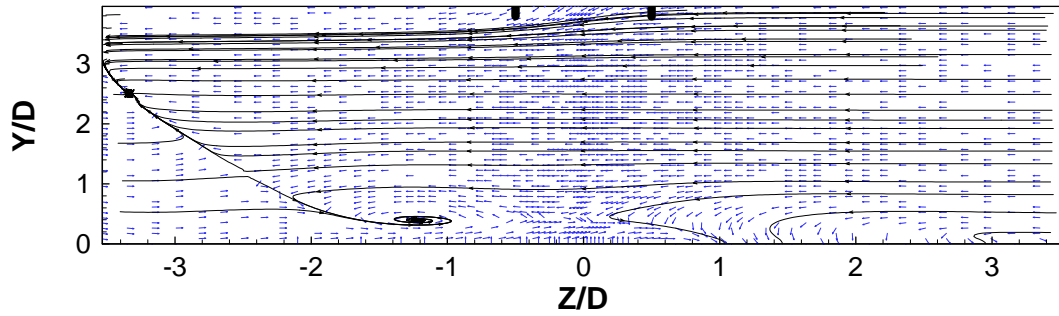


Figure 9. Engine Cf6-80a for U_i/U_∞ Max and $H/D_i=0.97$, $X=0.5XTOT$

And in the case of Cf6-6 engine there is the formation of three weak ground vortex at the same time, calling attention to the fact that two of them have a clockwise direction and not the third, as shown in Figure 10.

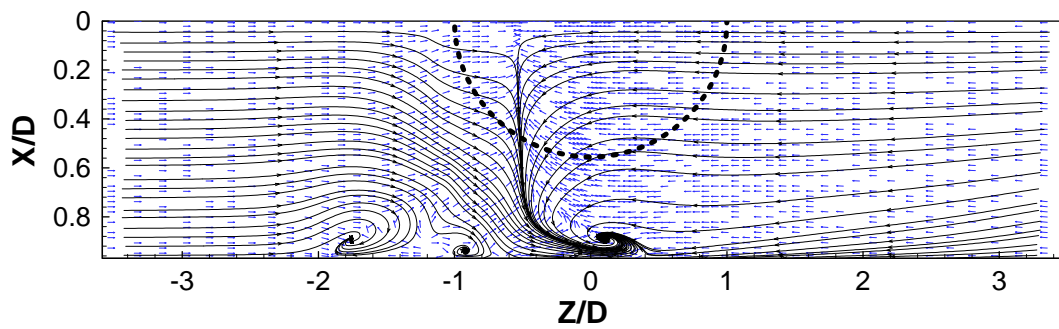


Figure 10. Engine Cf6-6 for U_i/U_∞ Max and $H/D_i=0.97$, $Y=0.05YTOT$

Engine	XZ	YZ	3D	Nº of vortex	V_i/V_∞	H/Di
cf6-50	X(2)	X		3	9.9	0.97
cf6-6	X(2)	X		3	9.9	0.97
cf6-80a	X(2)	X		3	9.9	0.97
cf6-80c2	X(2)	X		3	9.9	0.97
cf6-8oe1				0	9.9	0.97
cfm56-2				0	9.9	0.97
cfm56-3				0	9.9	0.97
cfm56-5a				0	9.9	0.97
cfm56-5b				0	9.9	0.97
cfm56-5c				0	9.9	0.97
cfm56-7				0	9.9	0.97
rb211-535e4				0	9.9	0.97
trent 500		X	X	2	9.9	0.97
trent 700		X	X	2	9.9	0.97
trent 800	X(2)	X		3	9.9	0.97
trent 1000	X	X		2	9.9	0.97
GE nx	X(2)	X		3	9.9	0.97

Table 3. Summary of results for the selected conditions.

For the case of table 3 we can again separate the results into three groups.

There is a group where in the XZ plane there are two vortical structures and one in the YZ plane. In the situation of the YZ plane four situations that occur should be described. The first is one in which the vortex changes direction of rotation as shown in Figure 11 and 12.

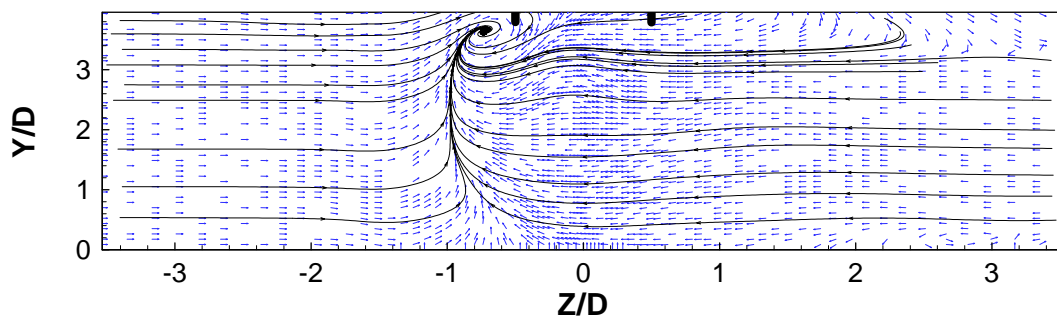


Figure 11. Engine Cf6-6 for $U_i/U_\infty=9.9$ and $H/Di=0.97$, $X=0.25XTOT$

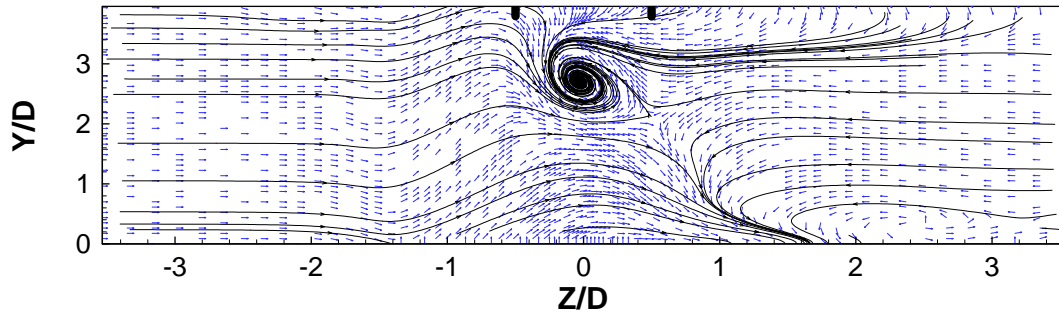


Figure 12. Engine Cf6-6 for $U_i/U_\infty=9.9$ and $H/D_i=0.97$, $X=0.5XTOT$

The second is that where the vortex with the clockwise rotation disappears from the first to the second graph causing increased disruption of the flow (Figure 13 and 14).

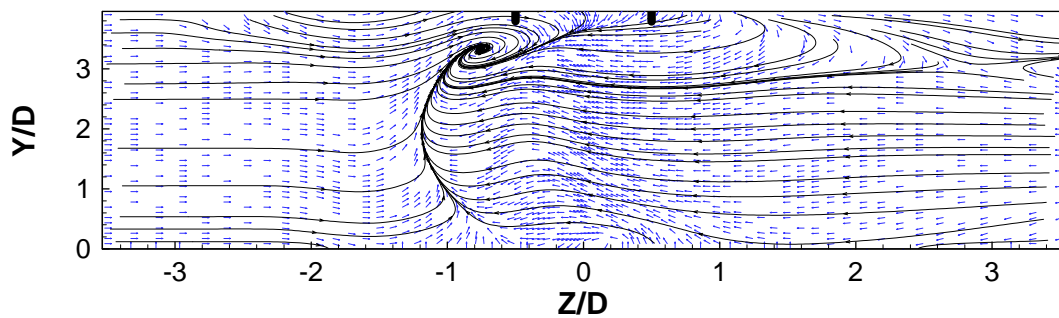


Figure 13. Engine Cf6-80c2 para $U_i/U_\infty=9.9$ e $H/D_i=0.97$, $X=0.25XTOT$

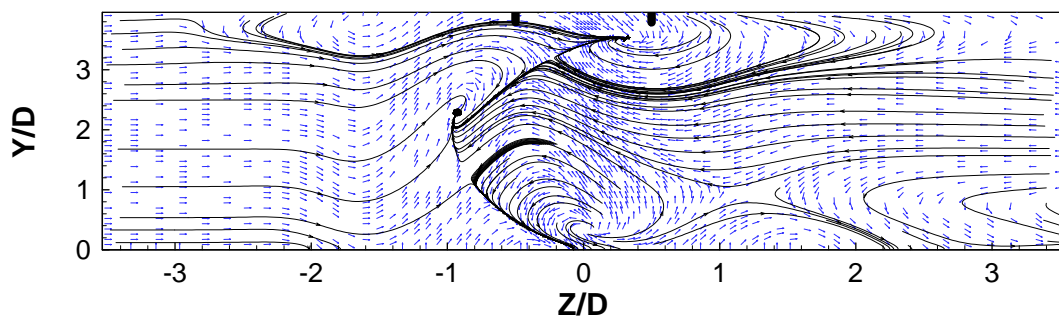


Figure 14. Engine Cf6-80c2 para $U_i/U_\infty=9.9$ e $H/D_i=0.97$, $X=0.5XTOT$

In the third situation where the case of the Trent 800 engine where the vortex occurs in the central area and far away from the engine (Figure 15).

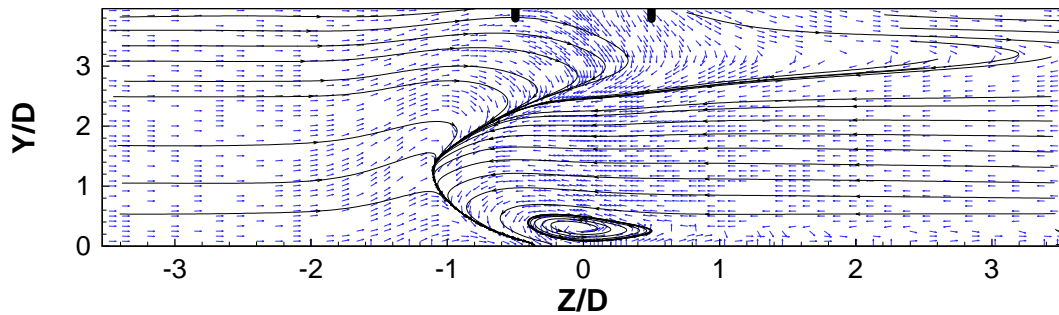


Figure 15. Engine Trent 800 for $U_i/U_\infty = 9.9$ and $H/D_i = 0.97$, $X = 0.5X_{TOT}$

In the latter situation we have the Ge-nx engine where you can see the vortex with a clockwise direction along the plane of the face of the engine and with the increase of X there is a Y/D decrease.

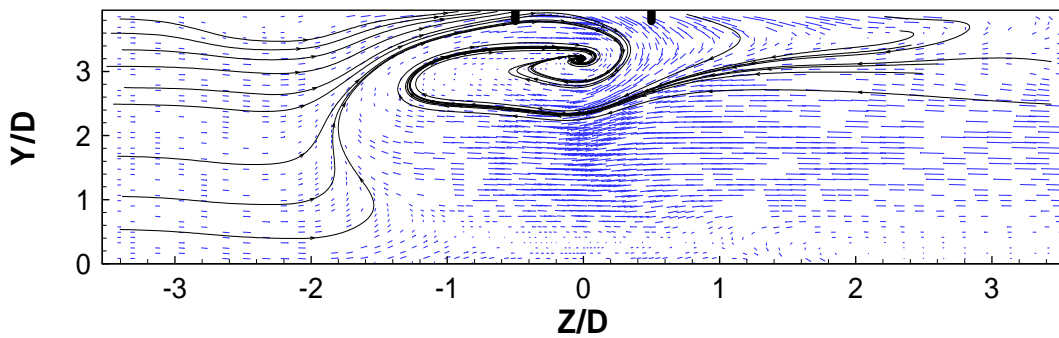


Figure 16. Engine GE-nx for $U_i/U_\infty = 9.9$ and $H/D_i = 0.97$, $X = 0.5X_{TOT}$

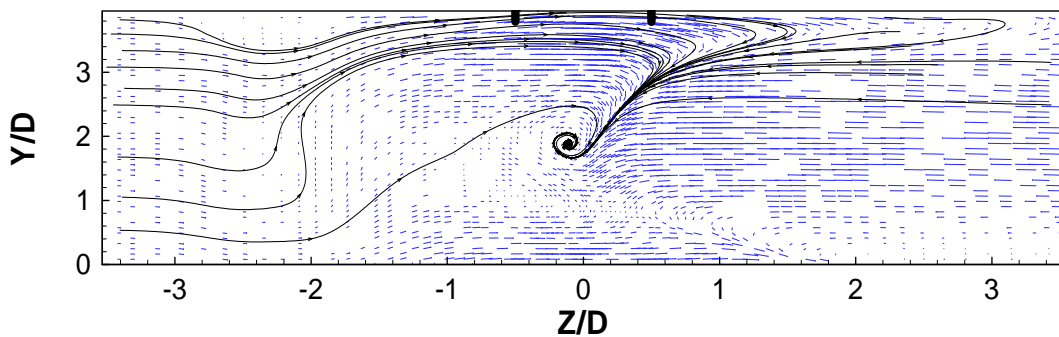


Figure 17. Engine Ge-nx for $U_i/U_\infty = 9.9$ and $H/D_i = 0.97$, $X = 0.75X_{TOT}$

In the YZ plane there are four situations to be described. In Figure 18 the position of the vortex is near the edge of the inlet nozzle. In Figure 19 we can see the difference in the position of the two vortex. In Figure 20 we can see the difference in intensity of vortex and in Figure 21 can verify the big difference compared to previous situations because there is a ground vortex of great intensity and another of weak intensity with an opposite rotation.

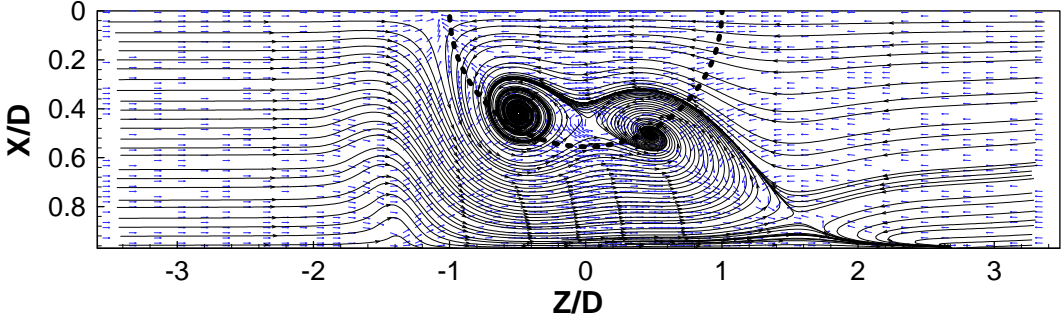


Figure 18. Engine Cf6-6 for $U_i/U_\infty = 9.9$ and $H/D_i = 0.97$, $Y = 0.5Y_{TOT}$

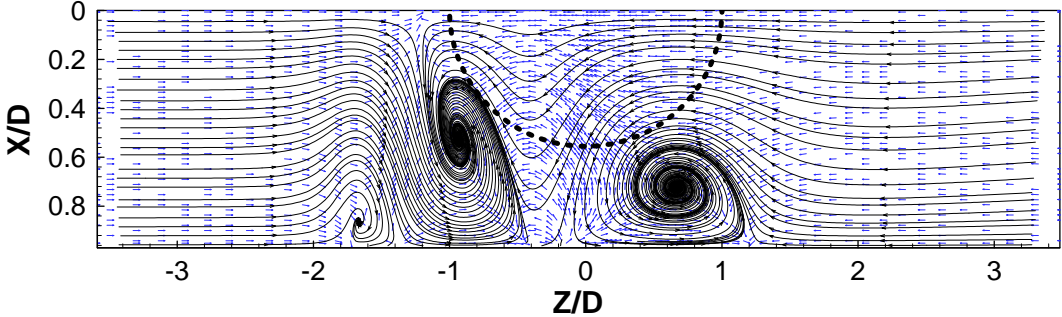


Figure 19. Engine cf6-80c2 for $U_i/U_\infty = 9.9$ and $H/D_i = 0.97$, $Y = 0.5Y_{TOT}$

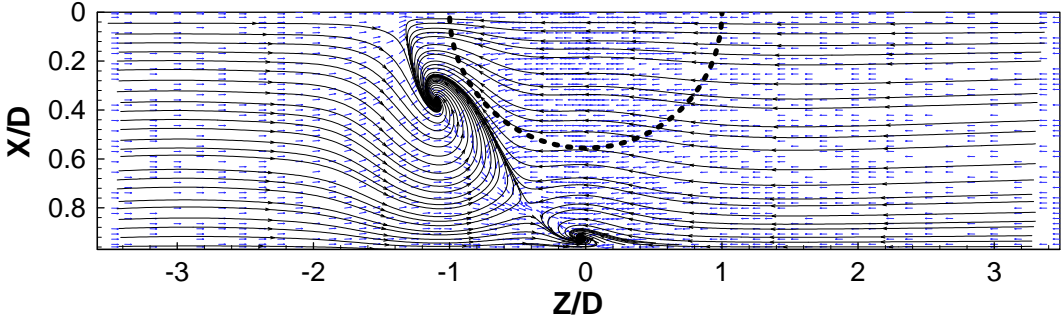


Figure 20. Engine Ge-nx for $U_i/U_\infty = 9.9$ and $H/D_i = 0.97$, $Y = 0.5Y_{TOT}$

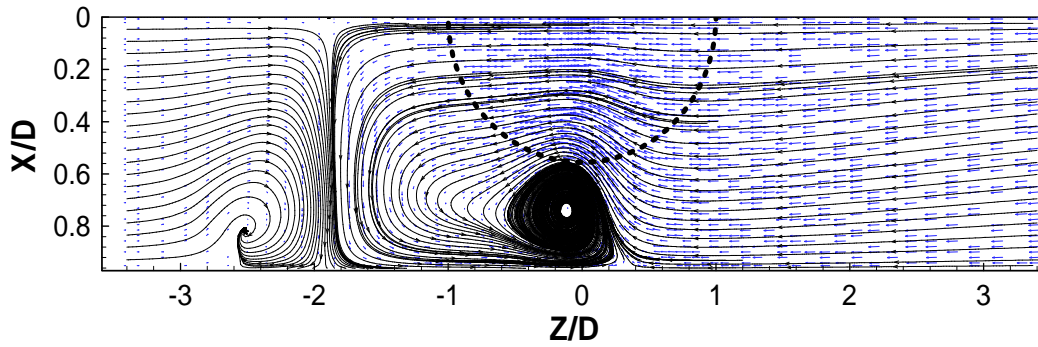


Figure 21. Engine Ge-nx for $U_i/U_\infty = 9.9$ and $H/D_i = 0.97$, $Y = 0.5Y_{TOT}$

In the case of the Trent 1000 engine there is a vortex in the YZ plane and another in the XZ plane. In relation to the XZ plane can see a vortex of high intensity near the inlet nozzle of the engine (Figure 22) and the YZ plane the vortex moves from one central location in the flow for a more lateral one and changing the direction of rotation (Figure 23 and 24).

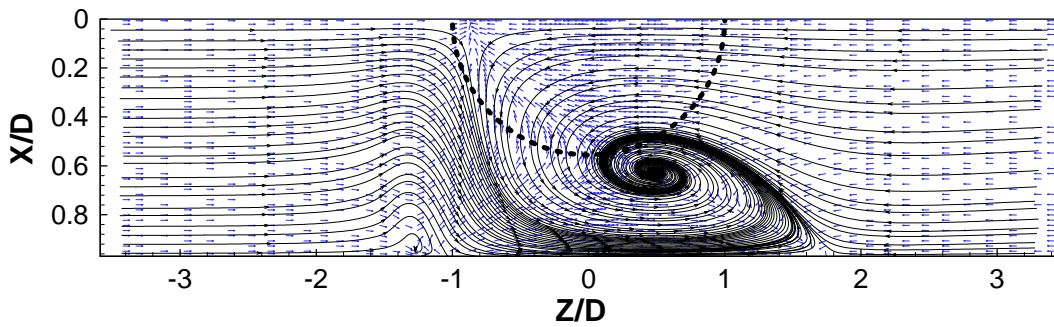


Figure 22. Engine Trent 1000 for $U_i/U_\infty = 9.9$ and $H/D_i = 0.97$, $Y = 0.5Y_{TOT}$

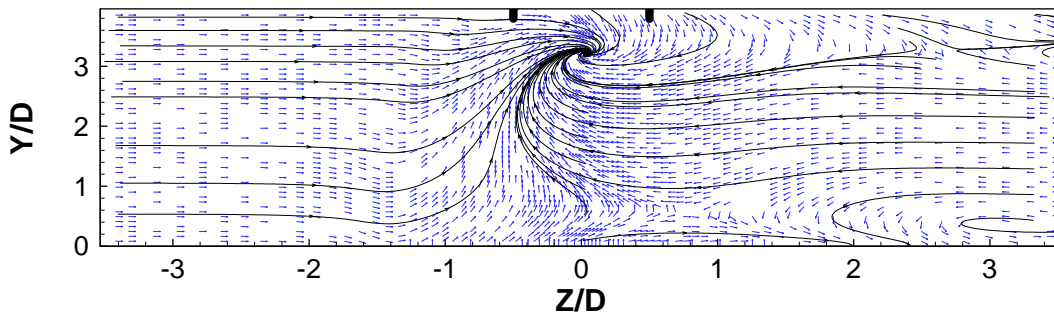


Figure 23. Engine Trent 1000 for $U_i/U_\infty = 9.9$ and $H/D_i = 0.97$, $X = 0.5X_{TOT}$

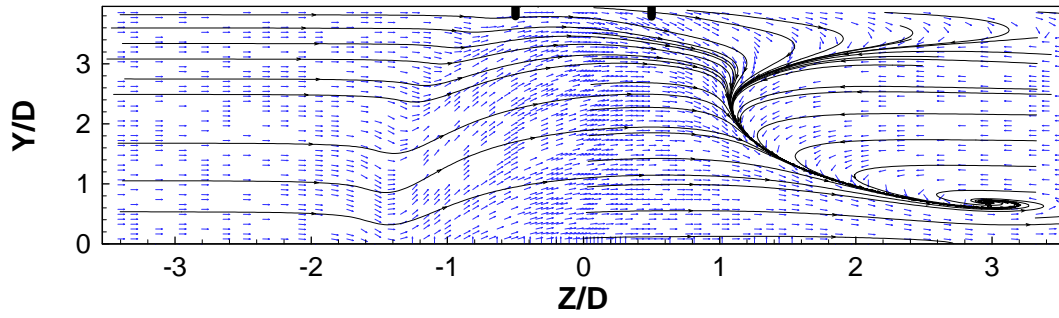


Figure 24. Engine Trent 1000 for $U_i/U_\infty=9.9$ and $H/D_i=0.97$, $X=0.75XTOT$

In the last group on Table 3 appears a result never observed until now, we can see in Figure 25 the return flow coming from the area downstream in the vicinity of $Y/D = 0$ and coming out near $Y/D = 10$.

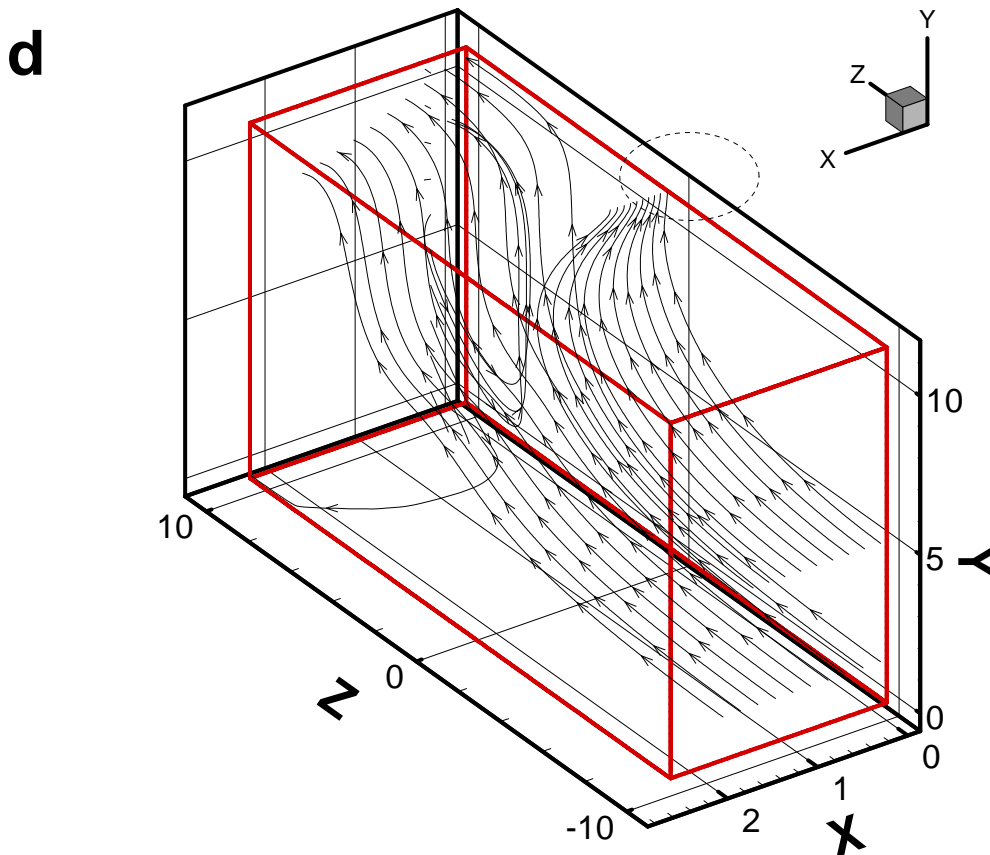


Figure 25. Engine Trent 500 for $U_i/U_\infty=9.9$ and $H/D_i=0.97$

In the YZ plane we can see a small vortex in the downstream of the nozzle (Figure 26).

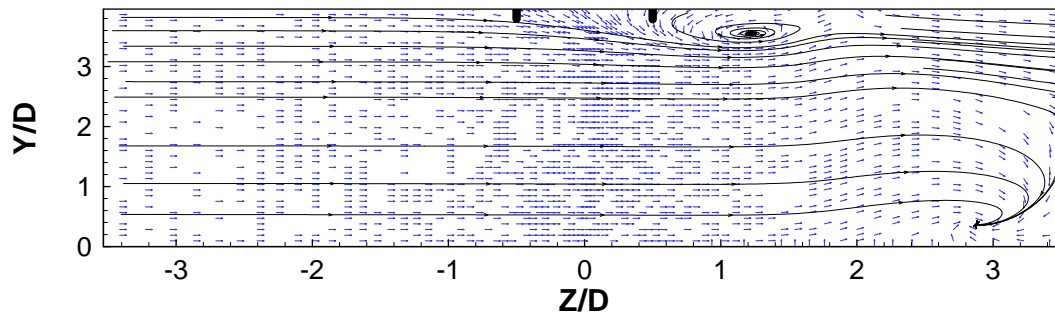


Figure 26. Engine Trent 500 for $U_i/U_\infty = 9.9$ and $H/D_i = 0.97$, $X = 0.5X_{TOT}$

Engine	XZ	YZ	3D	Nº of vortex	V_i/V_∞	H/Di
cf6-50				0	4.95	0.97
cf6-6				0	4.95	0.97
cf6-80a	X(2)	X		3	4.95	0.97
cf6-80c2				0	4.95	0.97
cf6-80e1				0	4.95	0.97
cfm56-2				0	4.95	0.97
cfm56-3				0	4.95	0.97
cfm56-5a				0	4.95	0.97
cfm56-5b				0	4.95	0.97
cfm56-5c				0	4.95	0.97
cfm56-7				0	4.95	0.97
rb211-535e4				0	4.95	0.97
trent 500				0	4.95	0.97
trent 700				0	4.95	0.97
trent 800				0	4.95	0.97
trent 1000				0	4.95	0.97
GE nx				0	4.95	0.97

Table 4. Summary of results for the selected conditions.

In table 4 we can verify the almost no vortex results with the only exception being the case the Cf6 80a engine, and his behavior is the same as described for the CF6-6 engine for the conditions in Table 3.

Engine	XZ	YZ	3D	Nº of vortex	V_i/V_∞	H/Di
cf6-50				0	9.9	1.2
cf6-6				0	9.9	1.2
cf6-80a				0	9.9	1.2
cf6-80c2	X(2)	X		3	9.9	1.2
cf6-80e1	X	X	X	3	9.9	1.2
cfm56-2			X	1	9.9	1.2
cfm56-3				0	9.9	1.2
cfm56-5a			X	1	9.9	1.2
cfm56-5b			X	1	9.9	1.2
cfm56-5c			X	1	9.9	1.2
cfm56-7				0	9.9	1.2
rb211-535e4			X	1	9.9	1.2
trent 500		X	X	2	9.9	1.2
trent 700				0	9.9	1.2
trent 800		X		1	9.9	1.2
trent 1000		X		1	9.9	1.2
GE nx		X		1	9.9	1.2

Table 5. Summary of results for the selected conditions.

Regarding the results of Table 5 we can check the increasing of vortical structures mentioned before and the decrease of ground vortex. In Table 5 we can see five relevant result sets, two vortex in the XZ plane and one in the YZ plane. A vortex in the XZ plane one in the YZ plane and one in 3D. A 3D one. One 3D and one in the YZ plane and finally one in the YZ plane.

For the first situation we have the CF6-80C2 engine with two vortex in XZ and one in YZ. In the YZ plane emerges a structure similar to that described in Figures 13 and 14, and in relation to the XZ plane again there are two structures that look similar to those in Figure 19.

In the second situation three structures are visible in XZ and YZ and another one in 3D. In XZ a vortex arises in the area downstream of the stream as it is clearly visible in Figure 27.

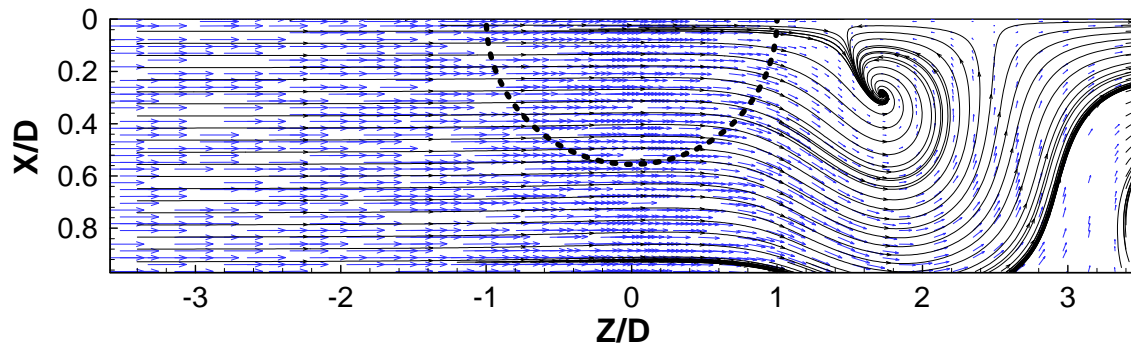


Figure 27. Engine Cf6-80c2 for $U_i/U_\infty = 9.9$ and $H/D_i = 1.2$, $Y = 0.5Y_{TOT}$

In the YZ plane appears a weak vortex and an area where the flow enters a plane coming from behind the plane of the face of the engine and follows in main the flow direction (Figure 28).

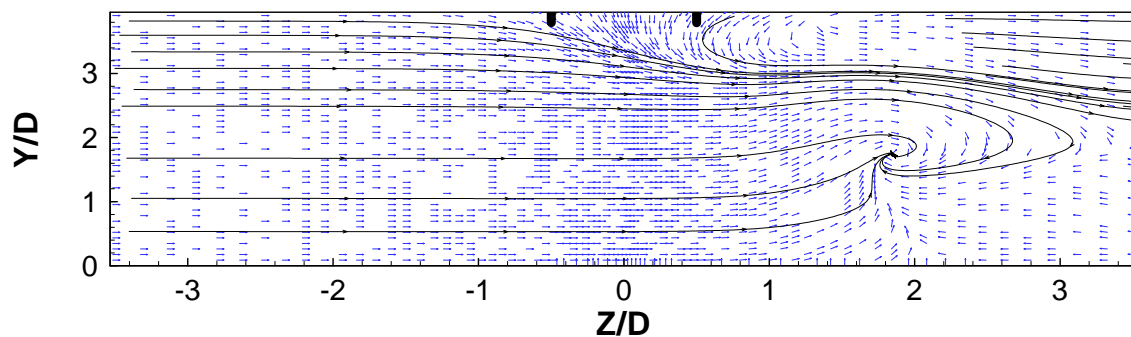


Figure 28. Engine Cf6-80c2 for $U_i/U_\infty = 9.9$ and $H/D_i = 1.2$, $X = 0.5X_{TOT}$

The 3D structure is identical to one already mentioned above in relation to Figure 25.

In the third set only arise visible structures in 3D perspective, which may be of three types. One already referenced above (Figure 15). A flow in the same area but weaker (Fig. 29) and a third is already well defined vortex and strong influence on the flow (Figure 30).

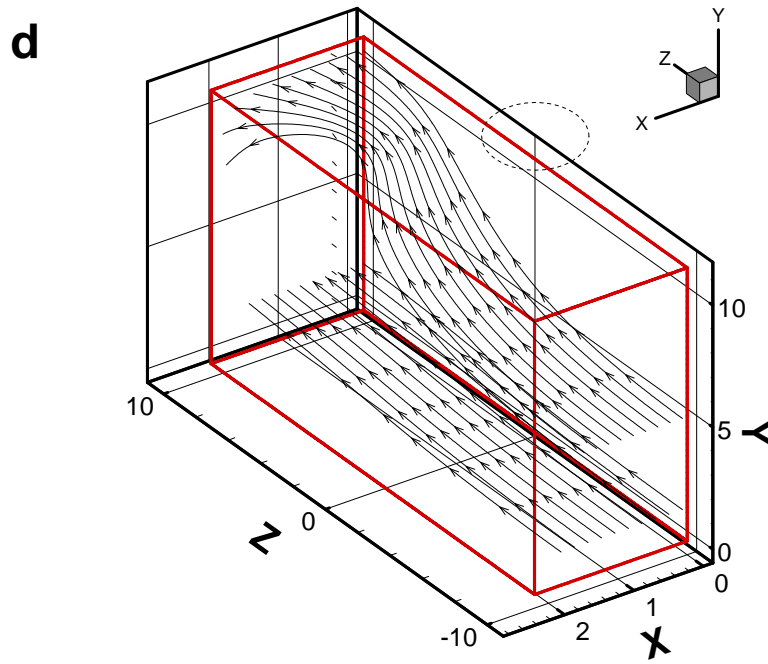


Figure 29. Engine Cf56-2 for $U_i/U_\infty = 9.9$ and $H/D_i = 1.2$

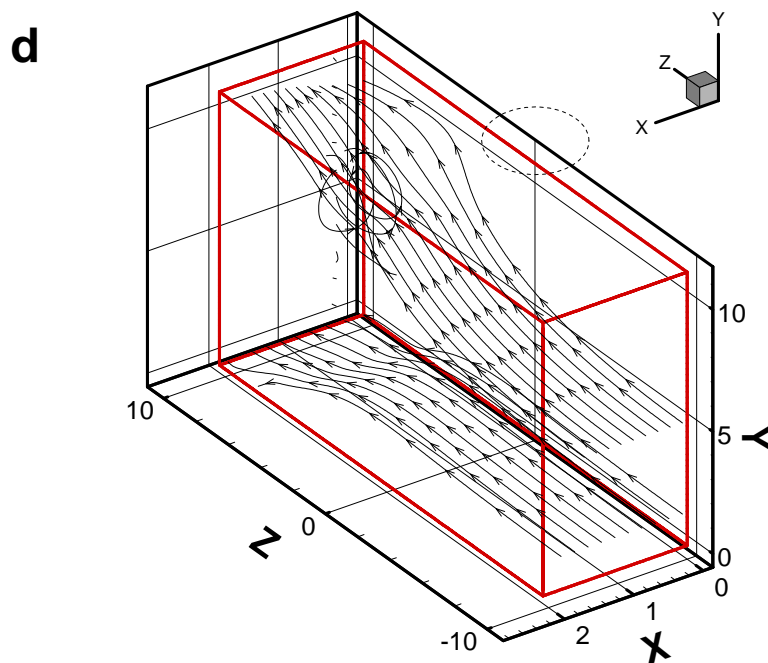


Figure 30. Engine Cf56-5c for $U_i/U_\infty = 9.9$ and $H/D_i = 1.2$

The fourth set of results is the Trent 500 where the structures are of the same kind found in Figure 25 and Figure 26.

Finally the fifth set of results which has only one YZ vortex, which is similar to others previously mentioned in terms of position but of greater intensity (Figure 31).

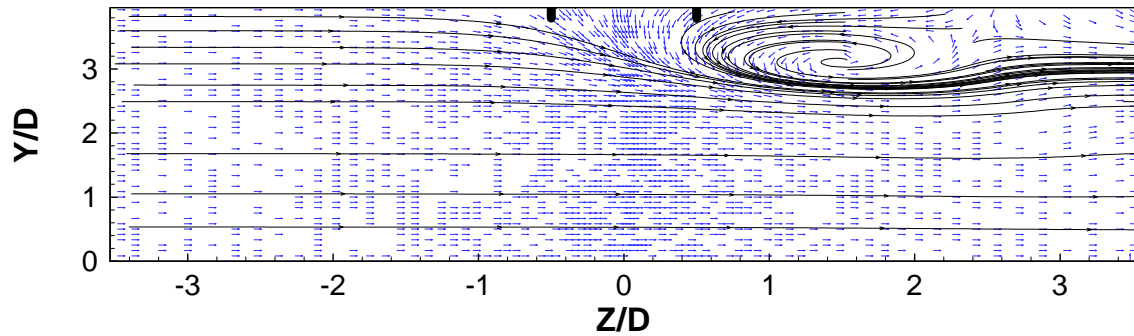


Figure 31. Engine Trent 800 for $U_i/U_\infty = 9.9$ and $H/D_i = 1.2$, $X = 0.5XTOT$

Figure 32 shows three-dimensional particle tracks for the Trent 900 and the GE nx engines for velocity ratios between the inlet and the crossflow, U_i/U_∞ , of 4.95, 9.8 and 19.8.

The vortex structure is detected for both engines for the highest velocity ratio (Fig. 32 e and f) with fluid being captured from both sides of the engine inlet that form a spiral directed towards the engine inlet.

For an intermediate velocity ratio of 9.9 the intake fluid is also being sucked upstream and downstream of the engine inlet but the spiral tendency is only noticeable for the case of the GE nx engine.

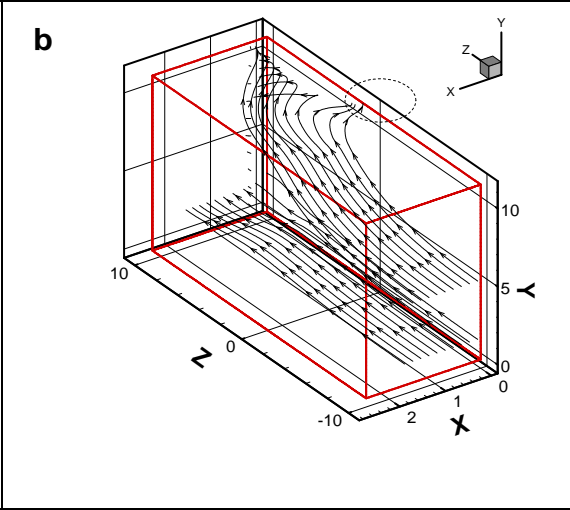
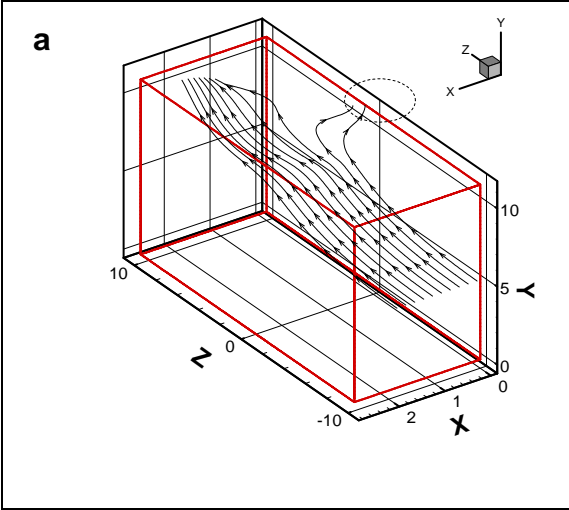
For the smallest velocity ratio ($U_i/U_\infty = 4.95$) the crossflow is less deflected by the engine for the Trent 900 case, while in the case of the GE nx is deviated towards the vertical plane of symmetry to form an outwards jet-like flow (in the opposite direction of the engine inlet flow).

Figure 32. Three-dimensional particle tracks.

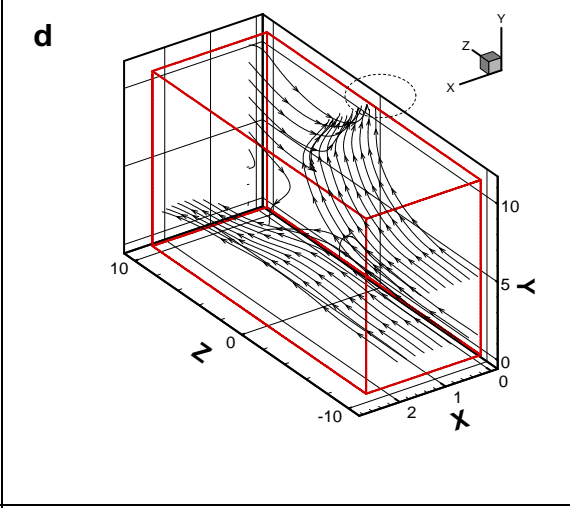
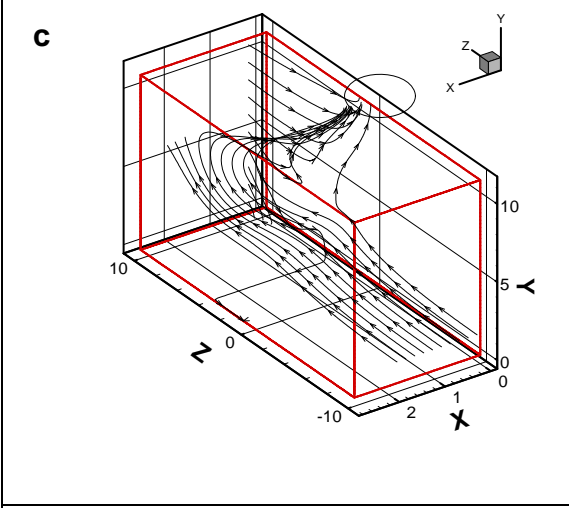
Trent 900

GE nx-1B64

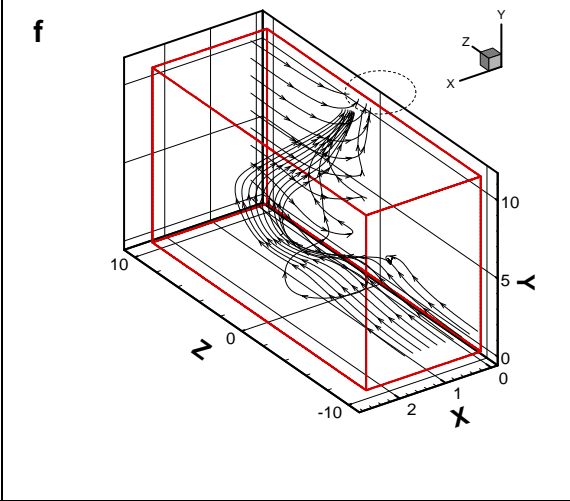
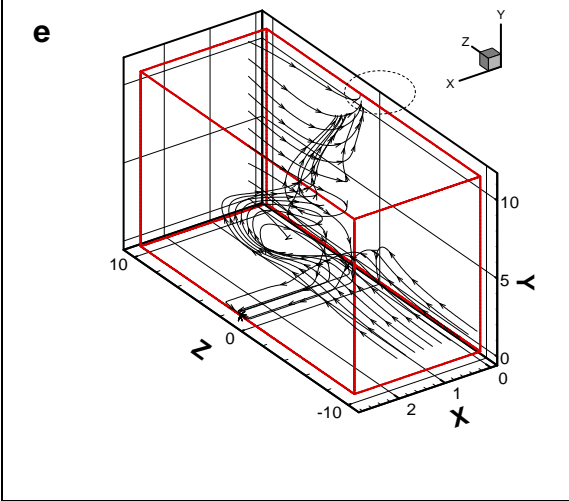
$U_i / U_\infty = 4.95$



$U_i / U_\infty = 9.9$



$U_i / U_\infty = 19.8$



The flow pattern described before is associated with typical ground pressure distributions that are shown in Fig. 33.

The static ground pressure nondimensionalized by the crossflow kinematic energy ($1/2\rho U_\infty^2$) is shown for the same conditions of Fig. 32 and both the Trent 900 and the GE nx-1B64 engines.

For the smallest velocity ratio (Fig. 33a and b) the negative pressure region is about the same size with intensity $(p - p_\infty)/(1/2\rho U_\infty^2) \approx -1.0$.

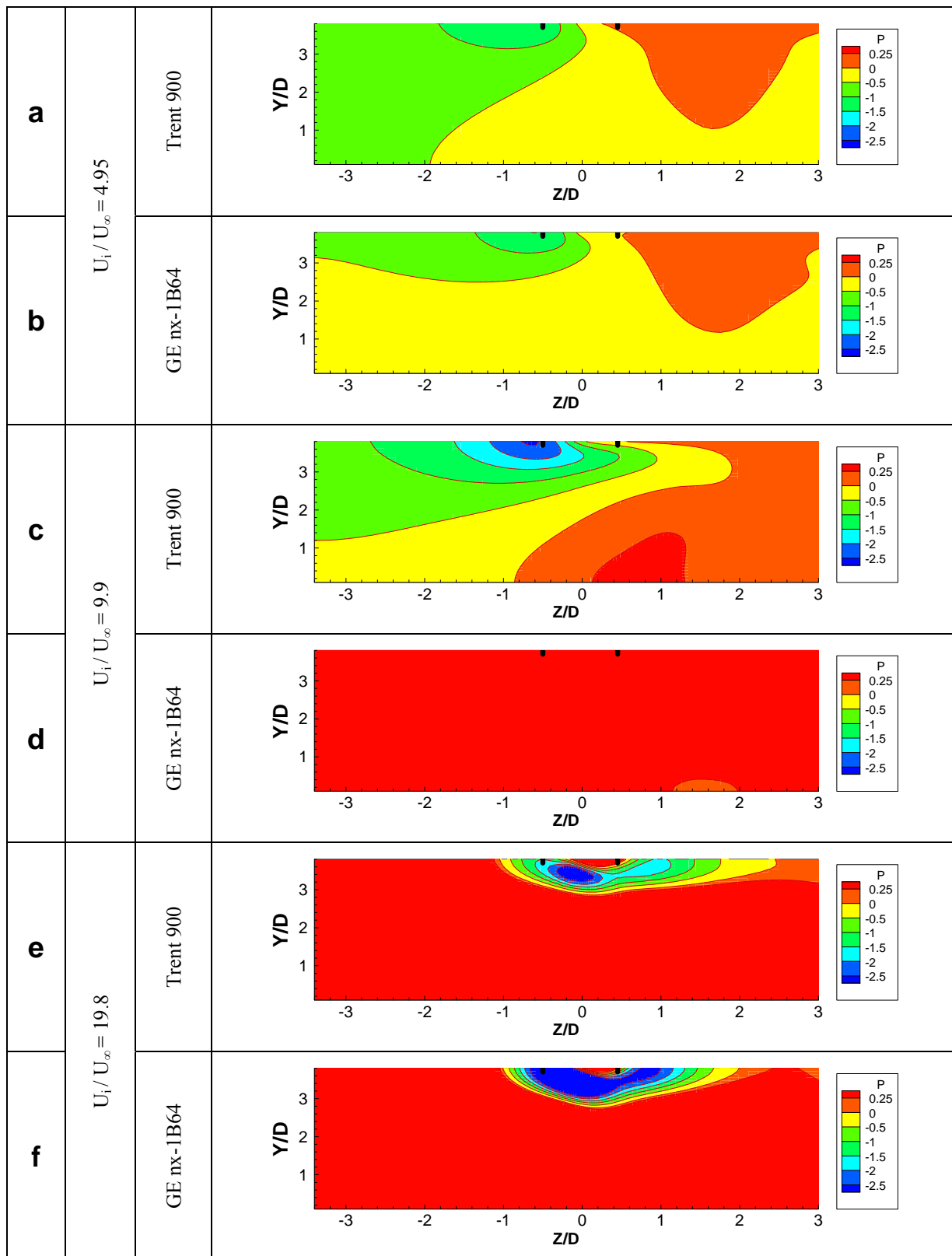
For a velocity ratio, U_i/U_∞ , of 9.9 (Fig. 33c and d), the negative region in the upstream side of the inlet becomes more intense with values of $(p - p_\infty)/(1/2\rho U_\infty^2)$ near -2.5, but in the downstream side the slight positive region also increases.

Finally, for the highest velocity ratio of $U_i/U_\infty=19.8$ (Fig. 5e and 5f) most of the ground floor is subjected to a relevant positive pressure, $0.25 < (p - p_\infty)/(1/2\rho U_\infty^2) < 0.5$, but a high suction region $(p - p_\infty)/(1/2\rho U_\infty^2) < -2.5$ in the inlet direction occurs.

The negative region is located in the upstream side for the Trent 900 case and its extension is about $3/4$ of the inlet diameter while for the case of the GE nx is considerably larger with a size slightly larger than one inlet diameter.

In spite of these negative values a small high pressure region can be observed in the downstream side which is associated with the tendency for the formation of a stagnation line and the corresponding stagnation point.

Figure 33. Ground pressure distribution $(p - p_\infty)/(1/2\rho U_\infty^2)$.

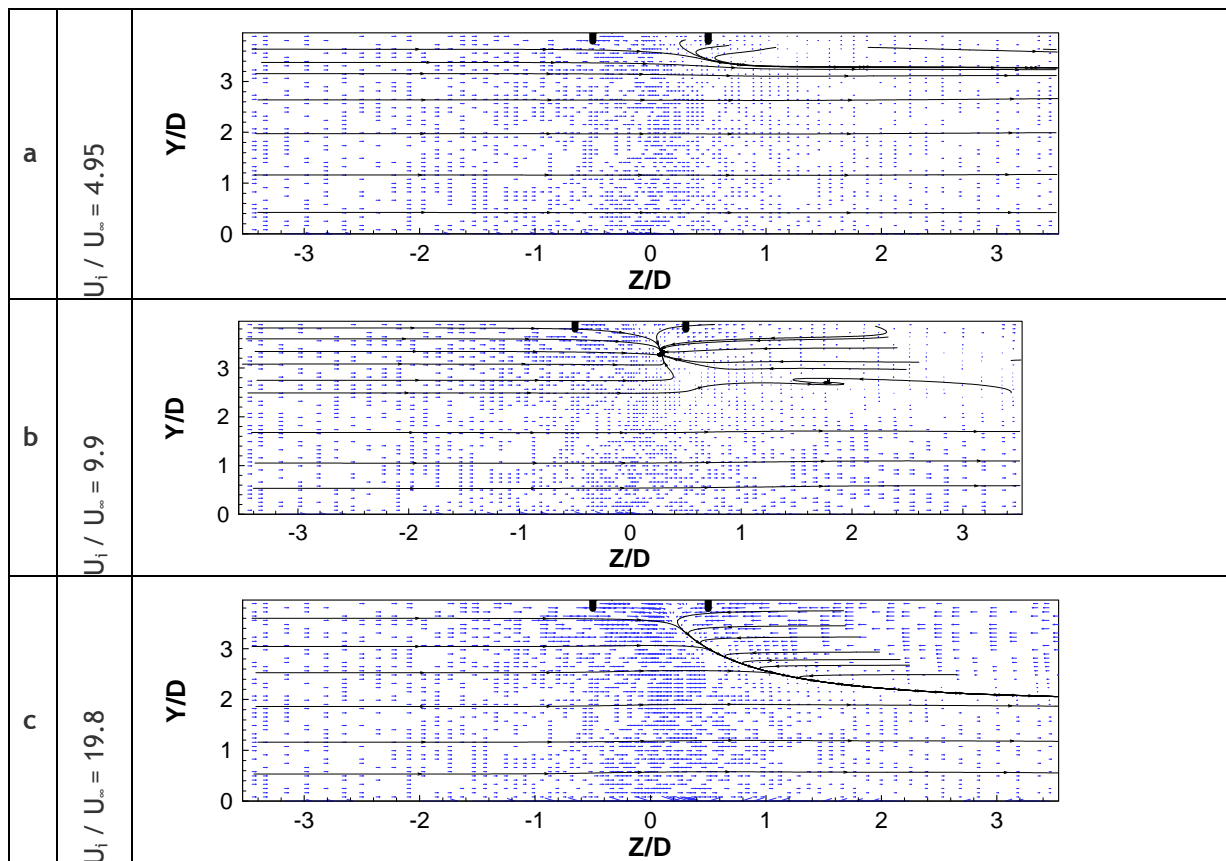


The formation of the ground vortex near the wall is further analyzed with the help of Fig. 34 which shows near wall velocity vectors and particle streaks for the GE nx-1B64 case.

The upstream and downstream flow converge to a line for the smallest and highest velocity ratio (Fig. 6a and c), while for $U_i/U_\infty=9.9$ (Fig. 34b) converge to a stagnation saddle point indicating the presence of the inlet vortex formation.

The main difference between the first and the third cases is the length of the diverted flow in the Y direction (horizontal parallel to the axis of the engine inlet) which increases from less than 1D to about twice with the velocity ratio.

Figure 34. Near wall velocity vectors and particle streaks for GE nx-1B64 test case.



For the intermediate velocity ratio $U_i/U_\infty=9.9$, Fig.35 shows the details of the flow pattern near the wall for the Trent 900 and the GE nx engines.

The stagnation point was detected for both engines but the misalignment with the crossflow is more pronounced for the GE nx.

For this velocity ratio the flow pattern is completely different from the observed for the lowest and highest velocity ratios with the flow converging to a single point at about $0.5D$ from the inlet plane.

It should be pointed out that from the three-dimensional perspectives of the flow (Fig. 32c and d) it is not possible to identify clearly any vertical structure that can be detected from this kind of near wall flow patterns.

Figure 35. Detail of the near wall velocity vectors and particle streaks for $U_i/U_\infty=9.9$.

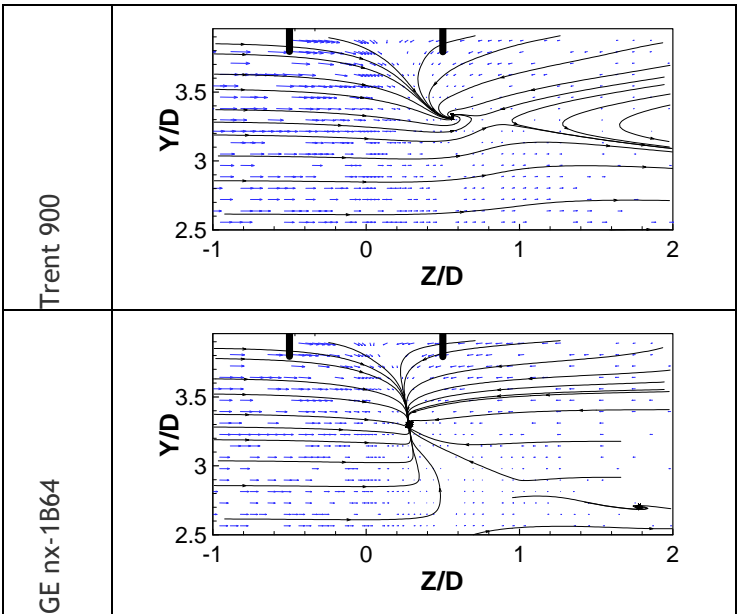


Figure 36 shows the typical flow development at the vertical plane near the engine inlet which assumes a similar pattern for all the test cases. The air is sucked in all directions towards the center of the inlet in a slightly distorted radial direction.

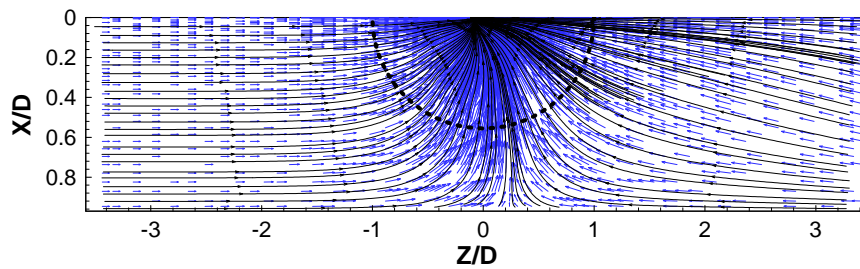


Figure 36. Typical Flow pattern at the vertical plane near the engine inlet for all the test cases (present results for Trent 900, $U_{in}/U_{\infty}=19.8$ and $h/D_i=0.97$, vertical plane parallel to the engine inlet at 56mm of distance).

Away from the engine inlet at a distance of $Y=5.6m$ measured along the axis, the flow is considerably different for each engine and test case (Fig. 37).

The core of a spiral can be identified for both the Trent 900 and the GE nx-1B64 engines, but its center is closer to the ground in the former case. It should be pointed out also that the cross-section of the flow is considerably larger for the case of the GE nx-1B64.

For the Trent 700 engine the vortex flow exists near the ground at the same plane but with an opposite sign (clockwise).

With a smaller velocity ratio ($U_i / U_{\infty} = 9.9$) the vortex flow becomes weaker (Fig. 37) and for the Trent 700 and cf6-80a totally disappears.

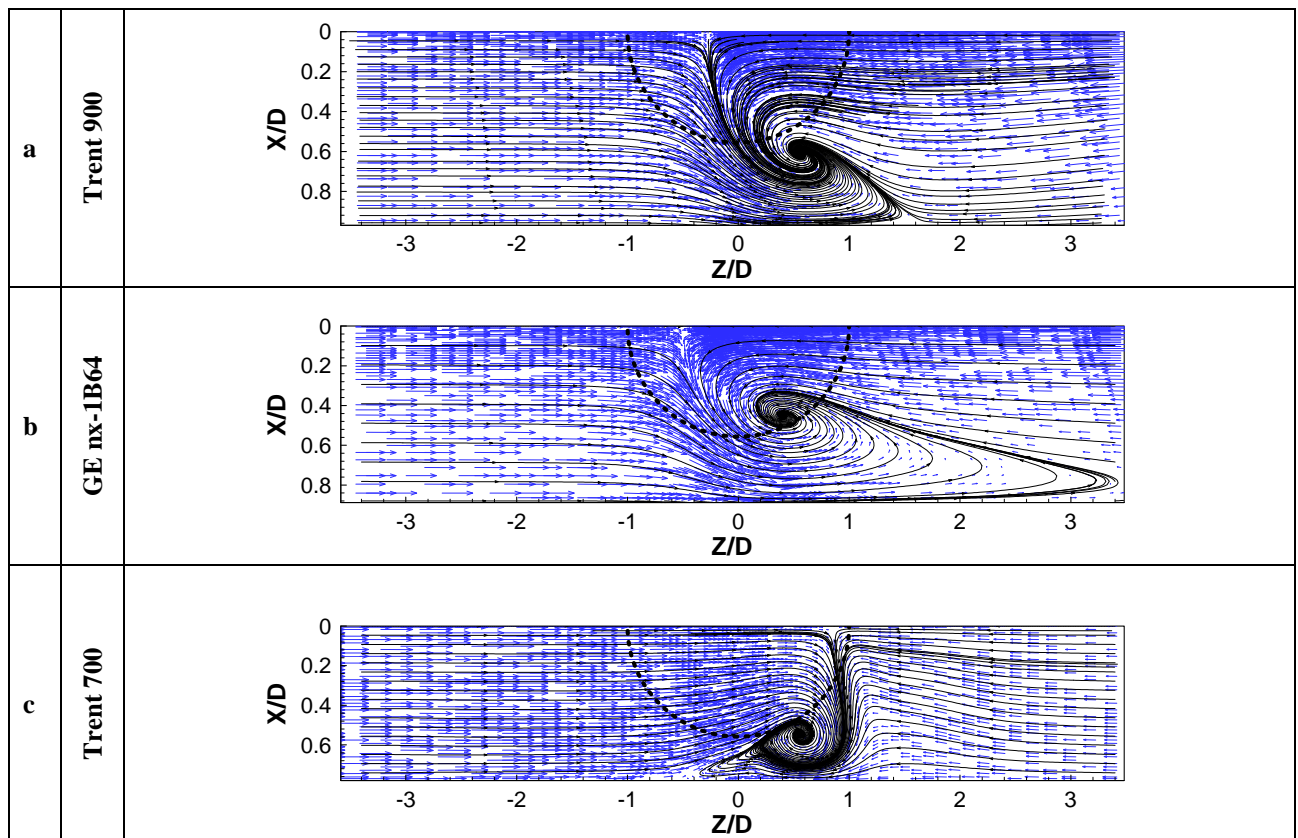


Figure 37. Velocity vectors and particle tracks in a vertical plane parallel to the engine inlet at 5.6m of distance ($U_i / U_\infty = 19.8$).

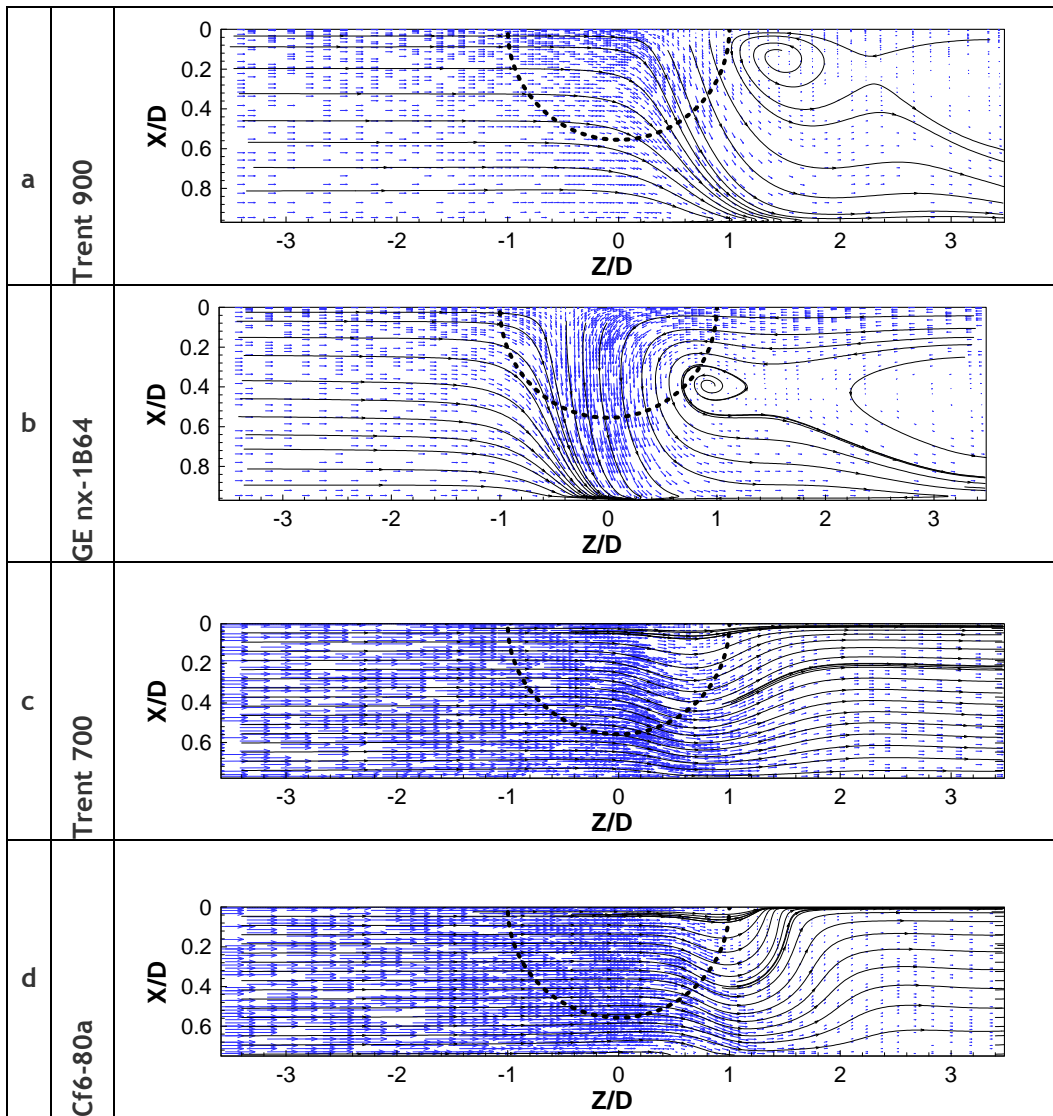


Figure 38. Velocity vectors and particle tracks in a vertical plane parallel to the engine inlet at 5.6m of distance ($U_i / U_\infty = 9.9$).

In these cases the crossflow is only slightly distorted but in general keeps its initial direction. For the Trent 900 and GE nx-1B64 the vortex flow can be already identified at 5.6m of distance from the inlet (Figs. 38a and b).

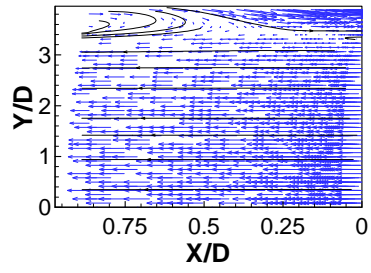


Figure 39. Velocity vectors and particle tracks in a vertical plane parallel to the engine axis at $Z=0.57D_i$

The existence of the trailing vortex was also investigated for all the test cases since it should be present all of the engine/test cases. Nevertheless, it was only clearly identified for some engine and more study is still needed.

Chapter 4

Conclusions

The present study has shown that the inlet flow of a gas turbine engine is strongly dependent on the velocity ratio between the inlet and any crosswind as well as on the diameter at its position above the ground.

Different engines have been studied and the formation of vortex was identified for all engines. The affected flow region was found to be considerably different in size. The trailing vortex could be clearly noticed for some engines.

Away from the inlet plane other types of complex vortical structures were identified that have different signs depending on the clearance distance of each particular engine and initial conditions.

By analyzing the different tables we can see the influence of inlet velocity and H in vortical structures.

We can conclude that for high inlet velocities vortical structures are almost exclusive to the XZ plane and with its decrease the formation of vortex passes through two stages one intermediate of an increase in vorticity at all levels and the second for low inlet velocities of almost absence of vortex.

With increased ground clearance to the shaft of the engines we see a change in the type of vortex that arise, with a decrease of it in the XZ plane, roughly the same number of structures in the YZ plane and big structures that are only possible to visualize in 3D perspective.

References

¹Hünecke, K. “Jet Engines: Fundamental of theory, design and operation”, Airlife publishing, UK, 1997.

²Mattingly, J.D., Heiser, W.H., Daley, D.H. “Aircraft Engine Design”, AIAA Education Series, New York, 1987.

³Mattingly, J.D. “Elements of Gas Turbine Propulsion”, Singapore: McGraw-Hill, 1996.

⁴Johns, C. “The Aircraft Engine Inlet Vortex Problem”, AIAA’s Aircraft Technology, Integrations and Operations (ATIO) 2002 Technical, 1-3rd 2002, Los Angles, California, AIAA Paper 2002-5894.

⁵Swainston, M. “Vortex Formation Near Intakes to Turbomachinery and Duct Systems”, Heat and Fluid Flow, Vol. 4, No. 2, 1974.

⁶Nakayama, A. & Jones, J. “Correlation for Formation of Inlet Formation”, AIAA Journal, Vol. 37, No. 4: Technical Notes, 1998.

⁷Motycka, D. & Walter, W. “An Experimental Investigation of Ground Vortex Formation During Reverse Thrust Operation”, AIAA Paper No. 75/1322, AIAA/SAE 11th Propulsion Conference, 1975

⁸Brix, S., Neuwerth, G. & Jacob, D. “The Inlet-Vortex System of Jet Engines Operating Near the Ground”, AIAA Paper 2000-3998, 2000

⁹De Siervi, F., Viguier, H., Greitzer, E. & Tan, C. “Mechanisms of Inlet Vortex Formation”, J. Fluid Mech., Vol. 124, pp. 173-207, 1982

¹⁰ Nakayama, A. & Jones, J. “Correlation for Formation of Inlet Formation”, AIAA Journal, Vol. 37, No. 4: Technical Notes, 1998.

¹¹Barata, J. M. M., Maneta, A.M., Silva, A.R.R. “ Numerical Study of Single Impinging Jets Through a Crossflow”, AIAA Paper no. 2009-4801, 45th AIAA/ASME/SAE/ASEE Joint propulsion Conference & Exhibit, Denver, CO, 2-5 Aug., 2009.

¹²Leonard, B. P. “A Stable and Accurate Convective Modelling Procedure Based on Quadratic Upstream Interpolation”, Computer Methods in Applied Mechanics and Engineering, Vol. 19, No.1, pp. 59-98, 1979

¹²Patankar, S. V. and Spalding, D. B. "A Calculation Procedure for Heat, Mass and Momentum Transfer in Three- Dimensional Parabolic Flows", *International Journal of Heat and Mass Transfer*, Vol. 15, No. 10, pp. 1787-1805, 1972.